Supplementary Figure 1

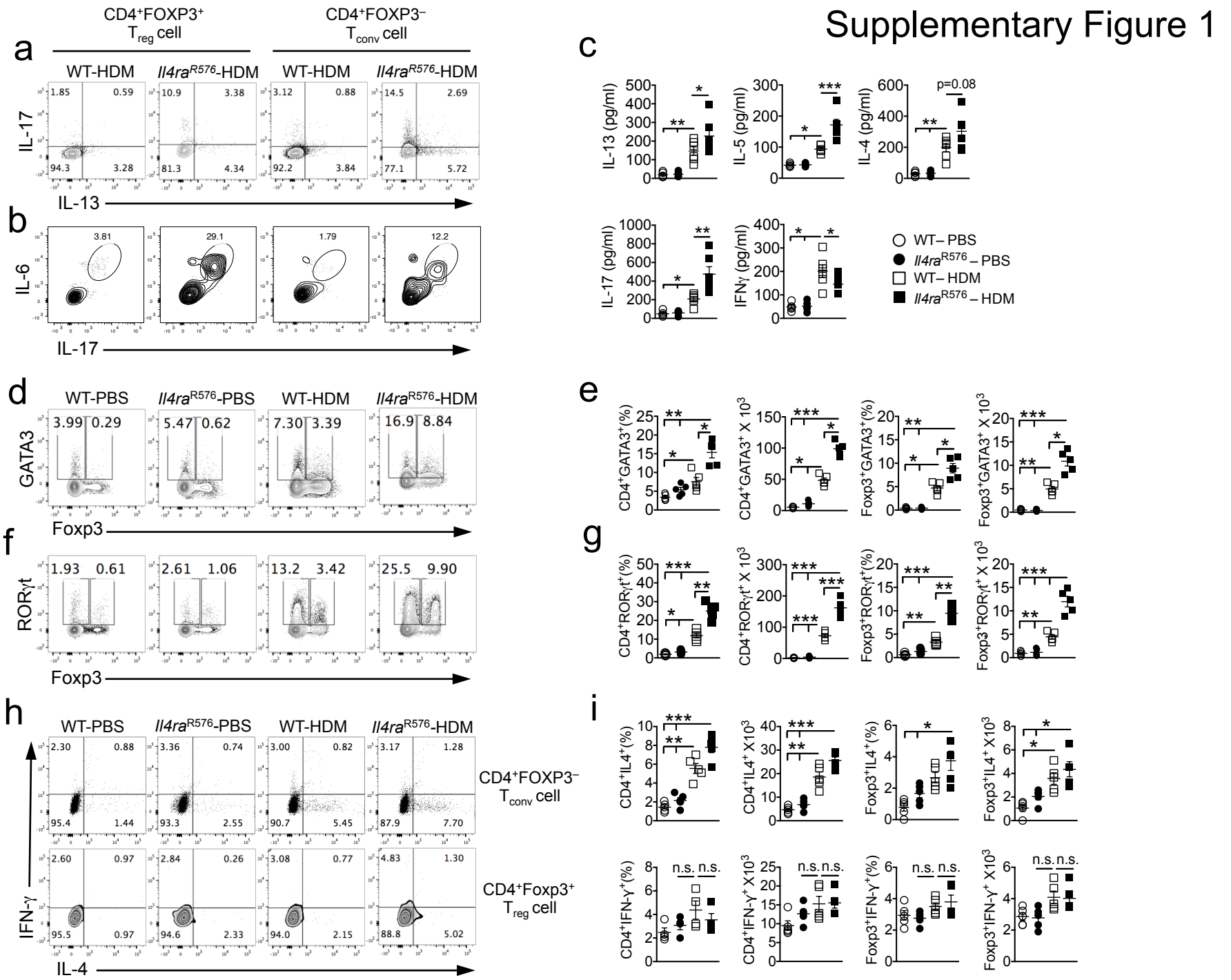

Supplementary Figure 2

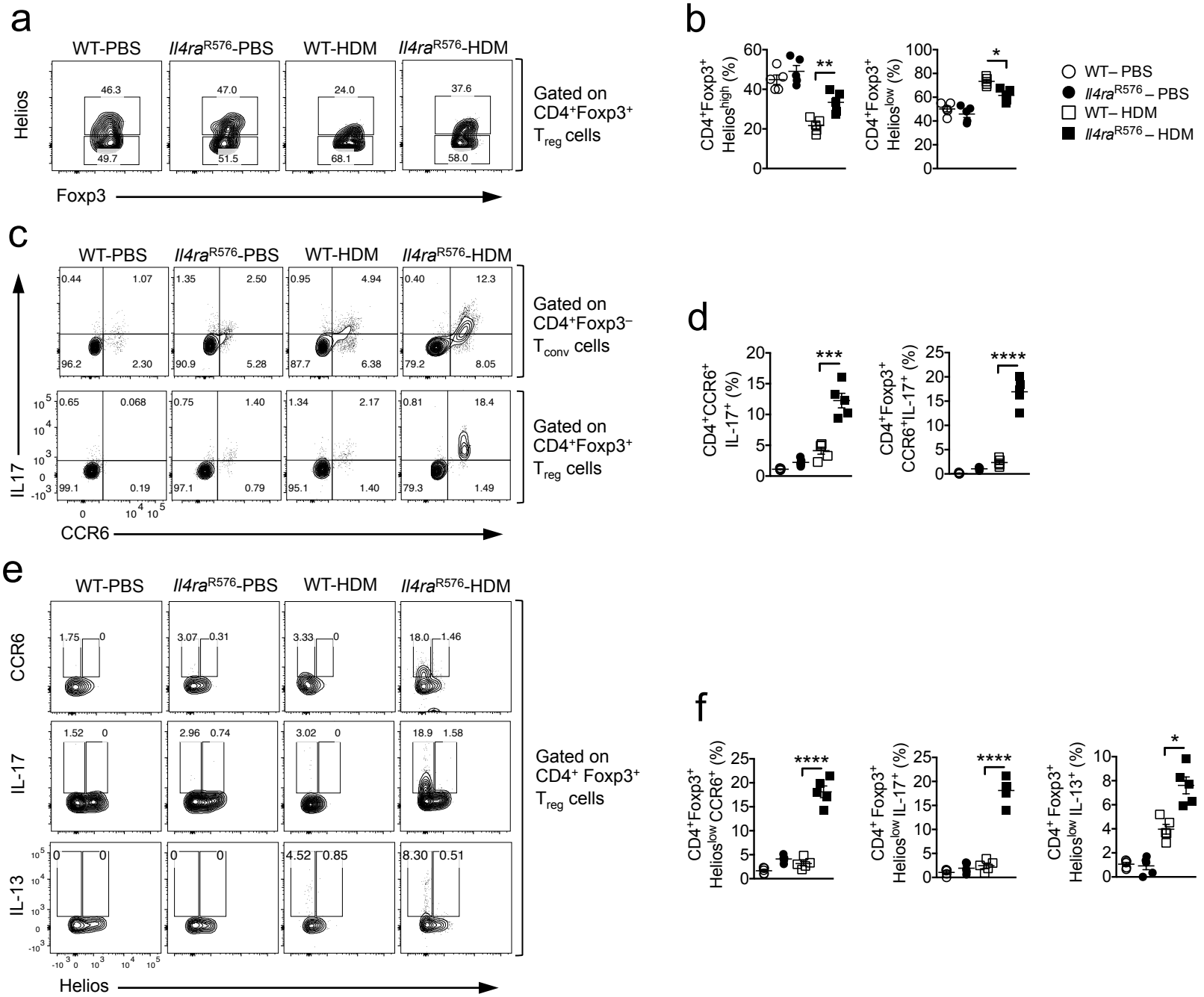

Supplementary Figure 3

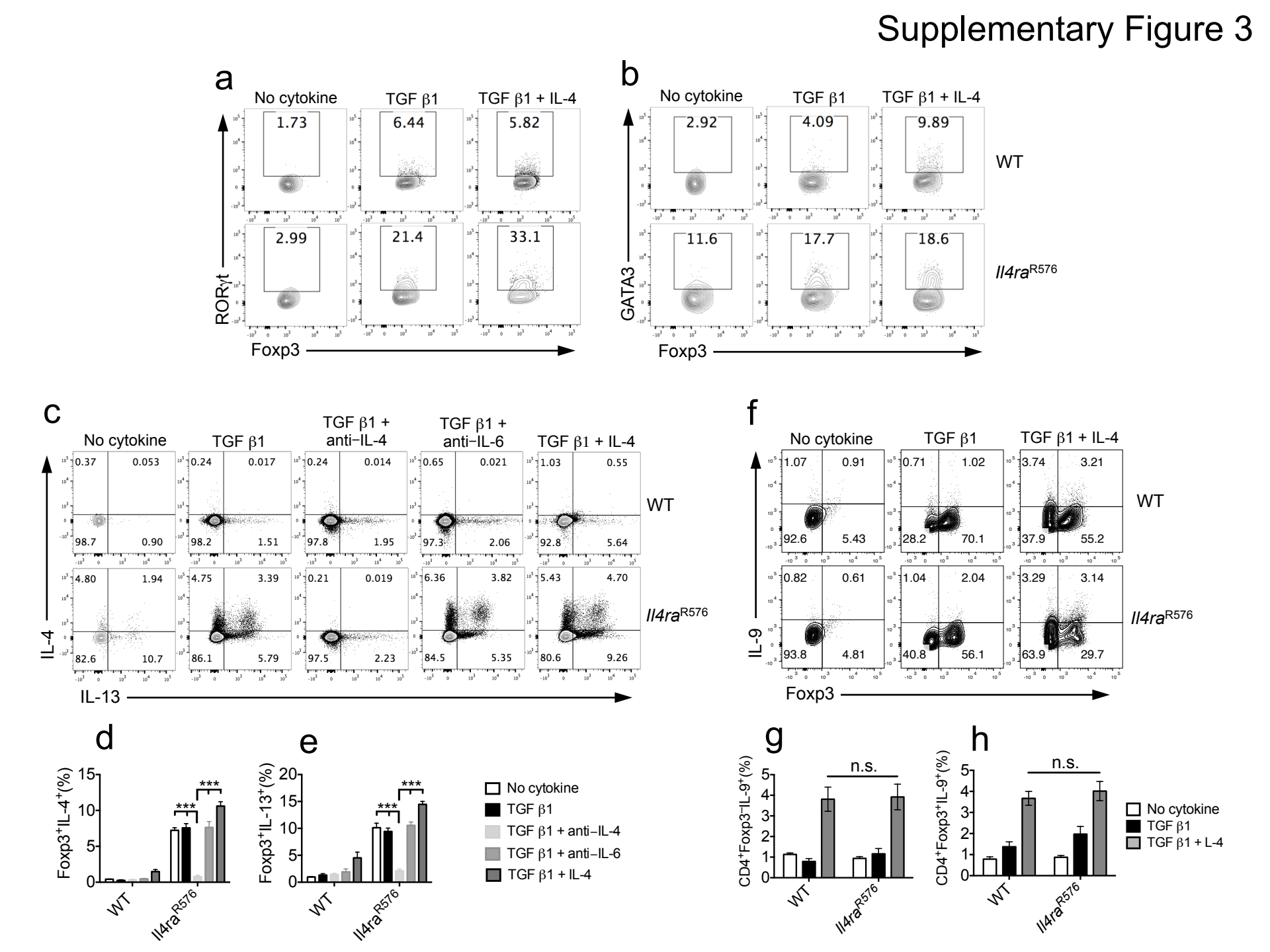

Supplementary Figure 4

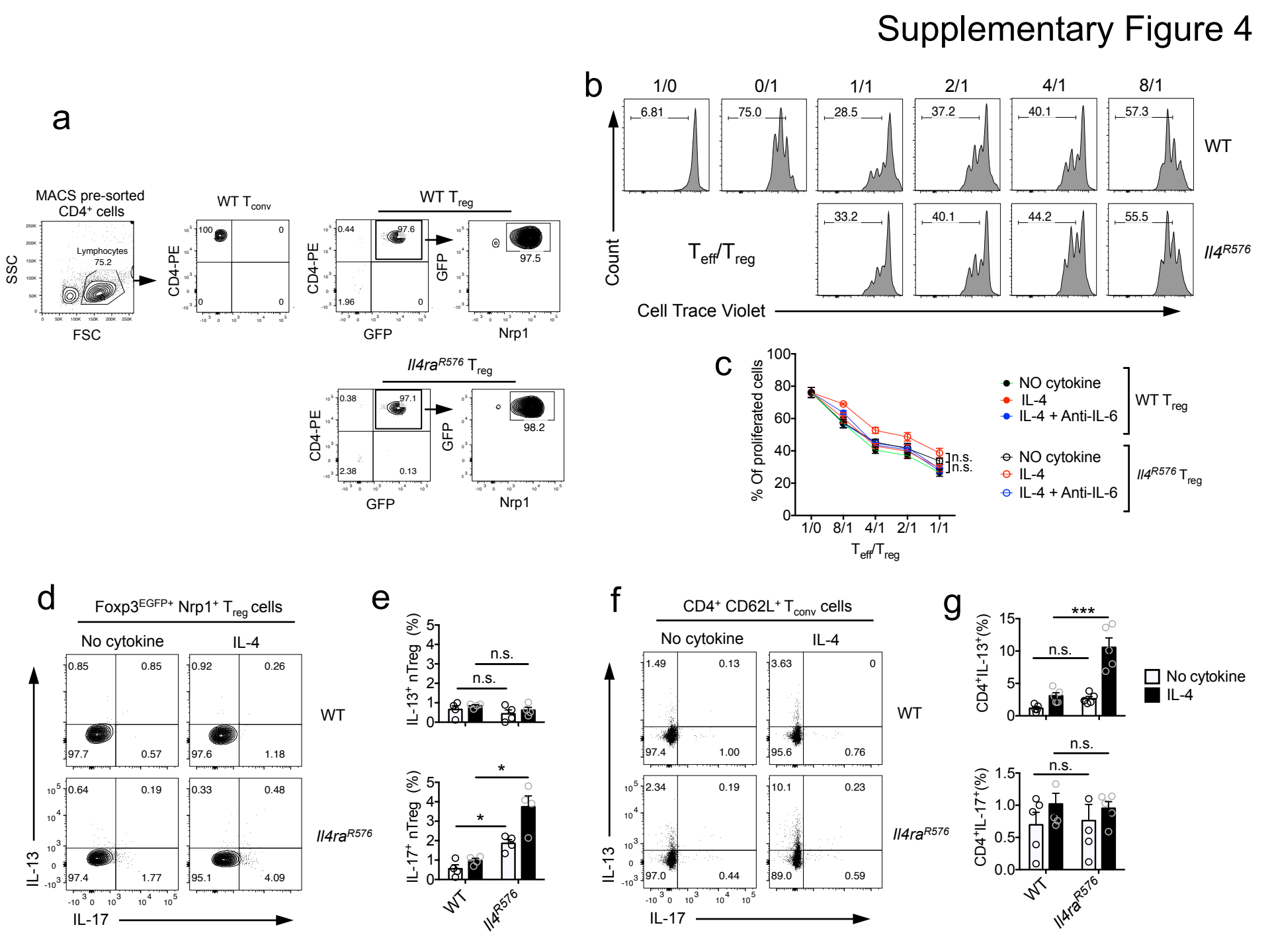

Supplementary Figure 5

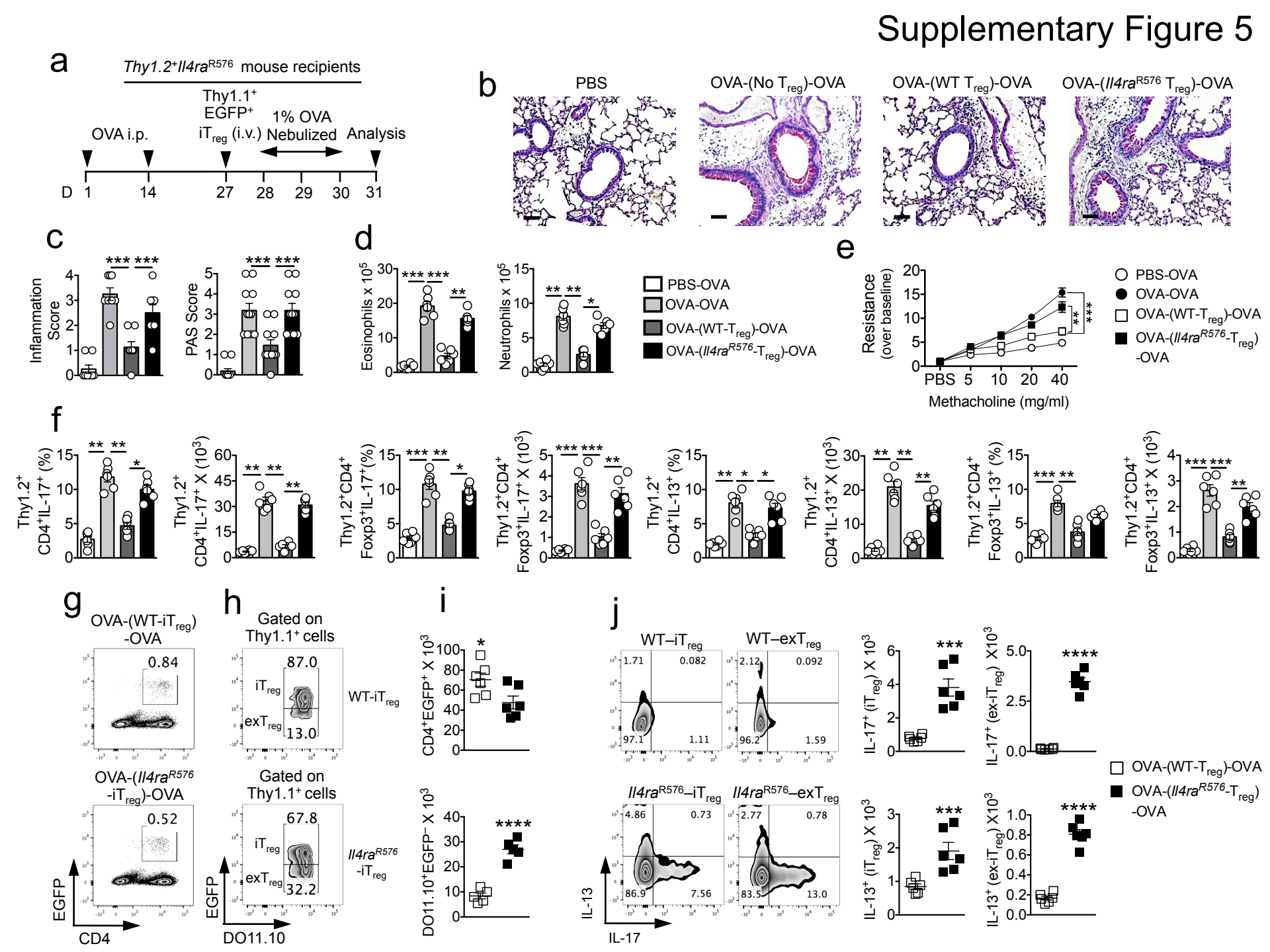

Supplementary Figure 6

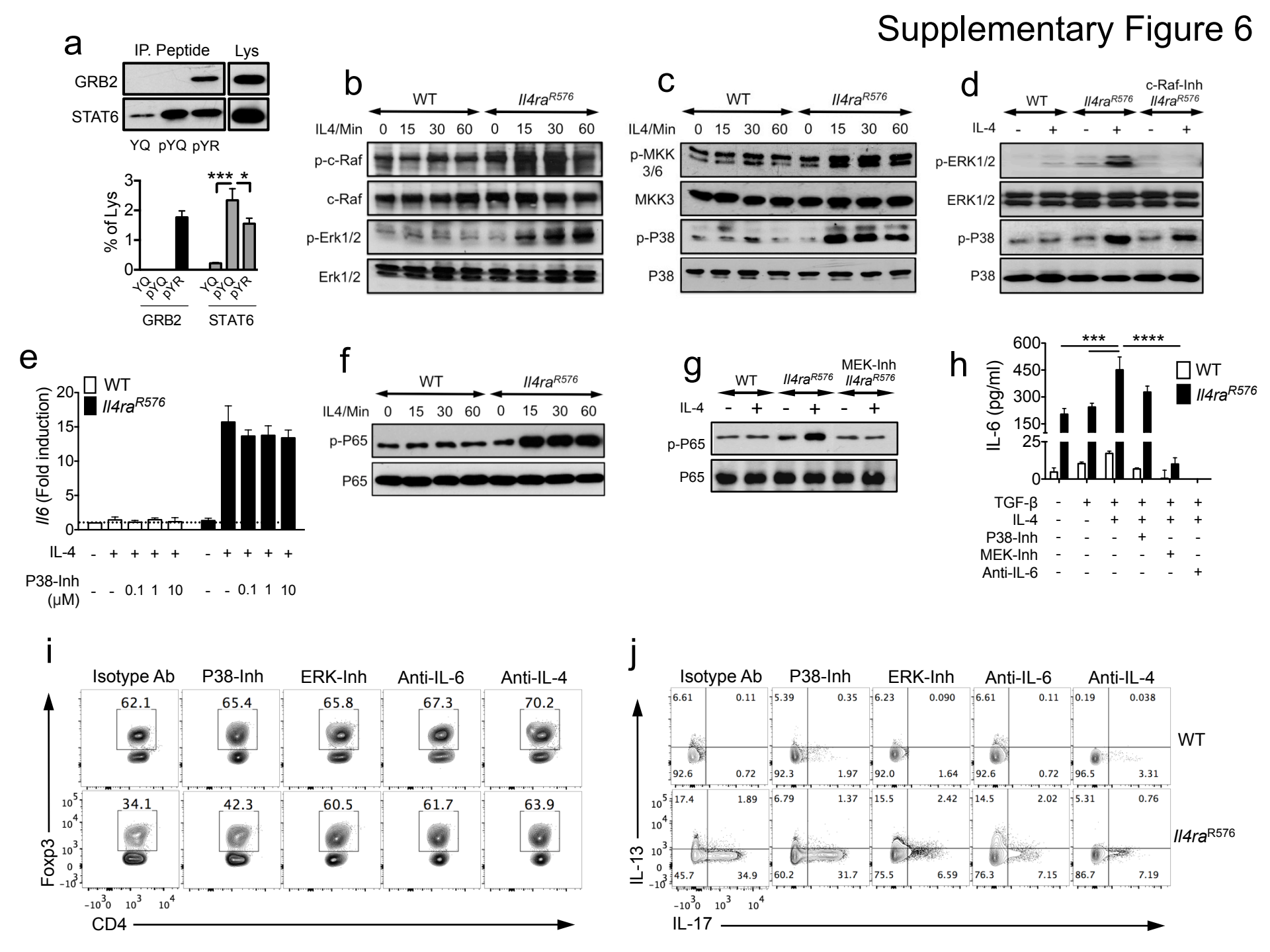

Supplementary Figure 7

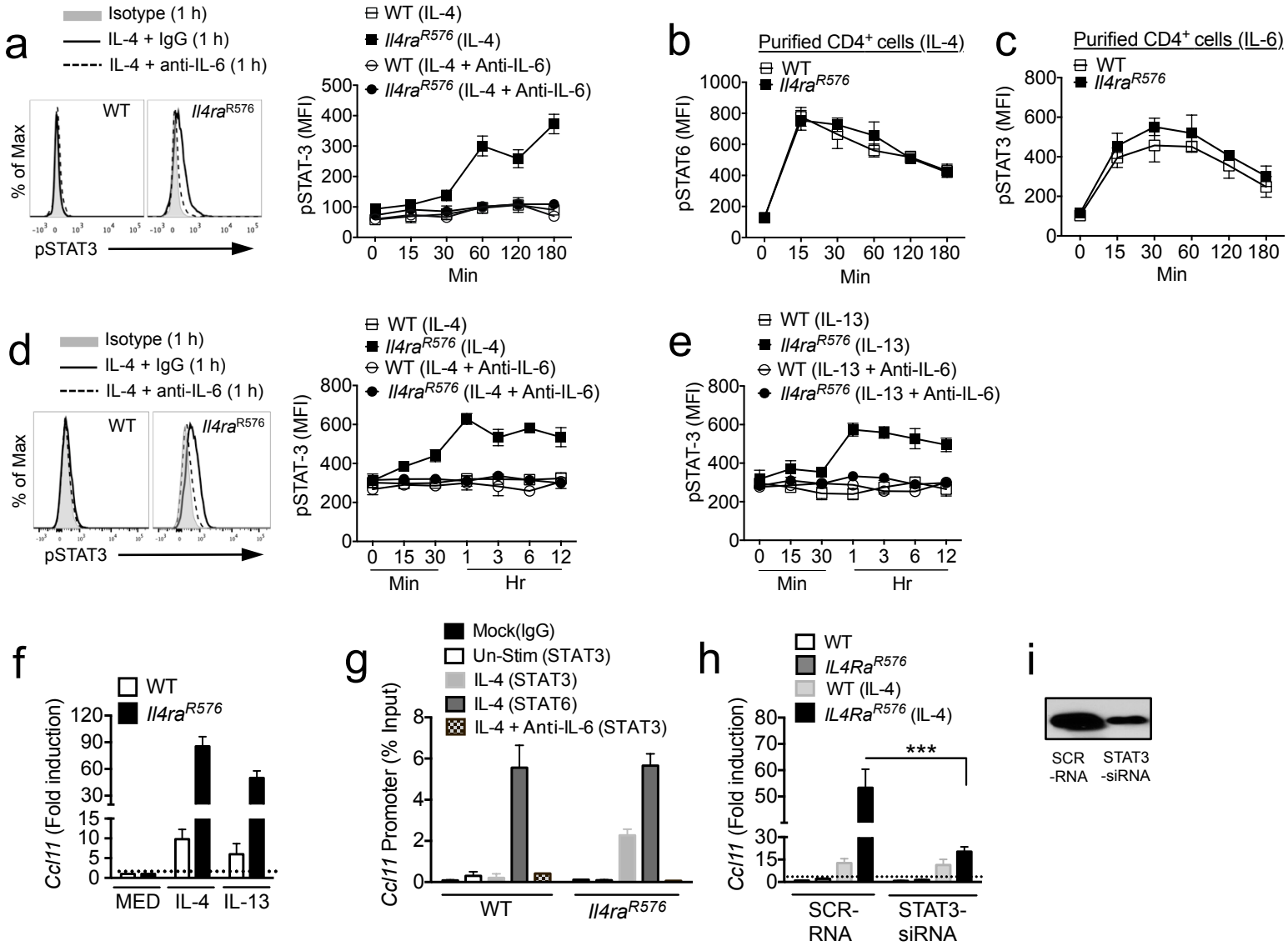

Supplementary Figure 8

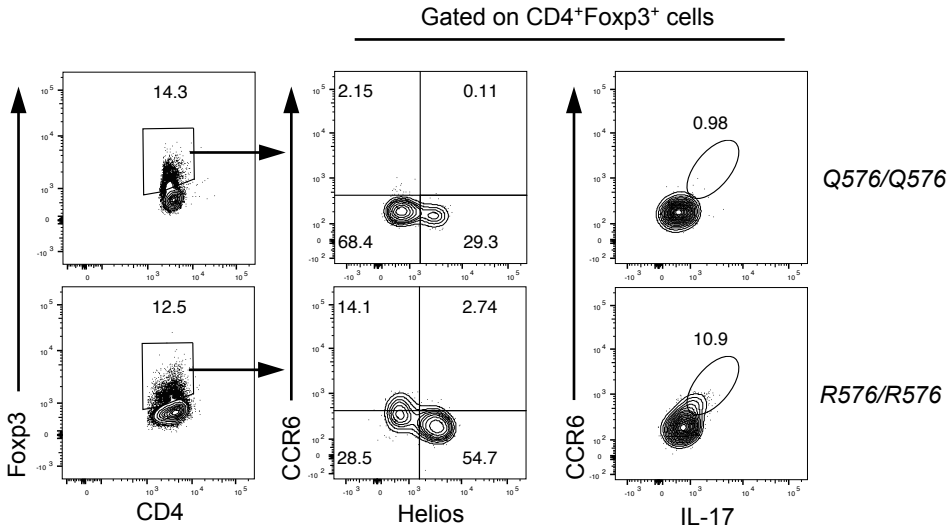

Supplementary Figure 9

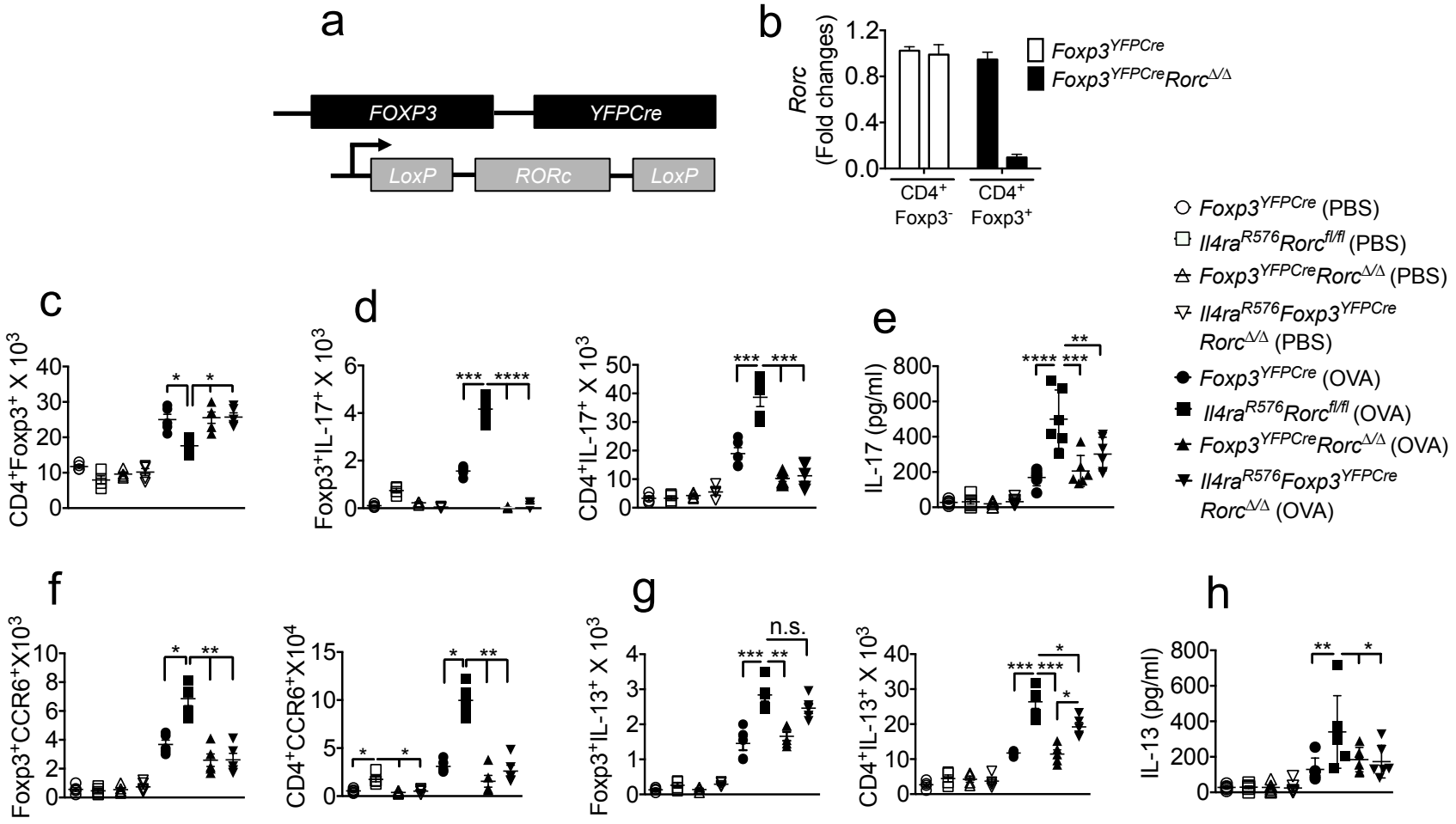

Supplementary Figure 10

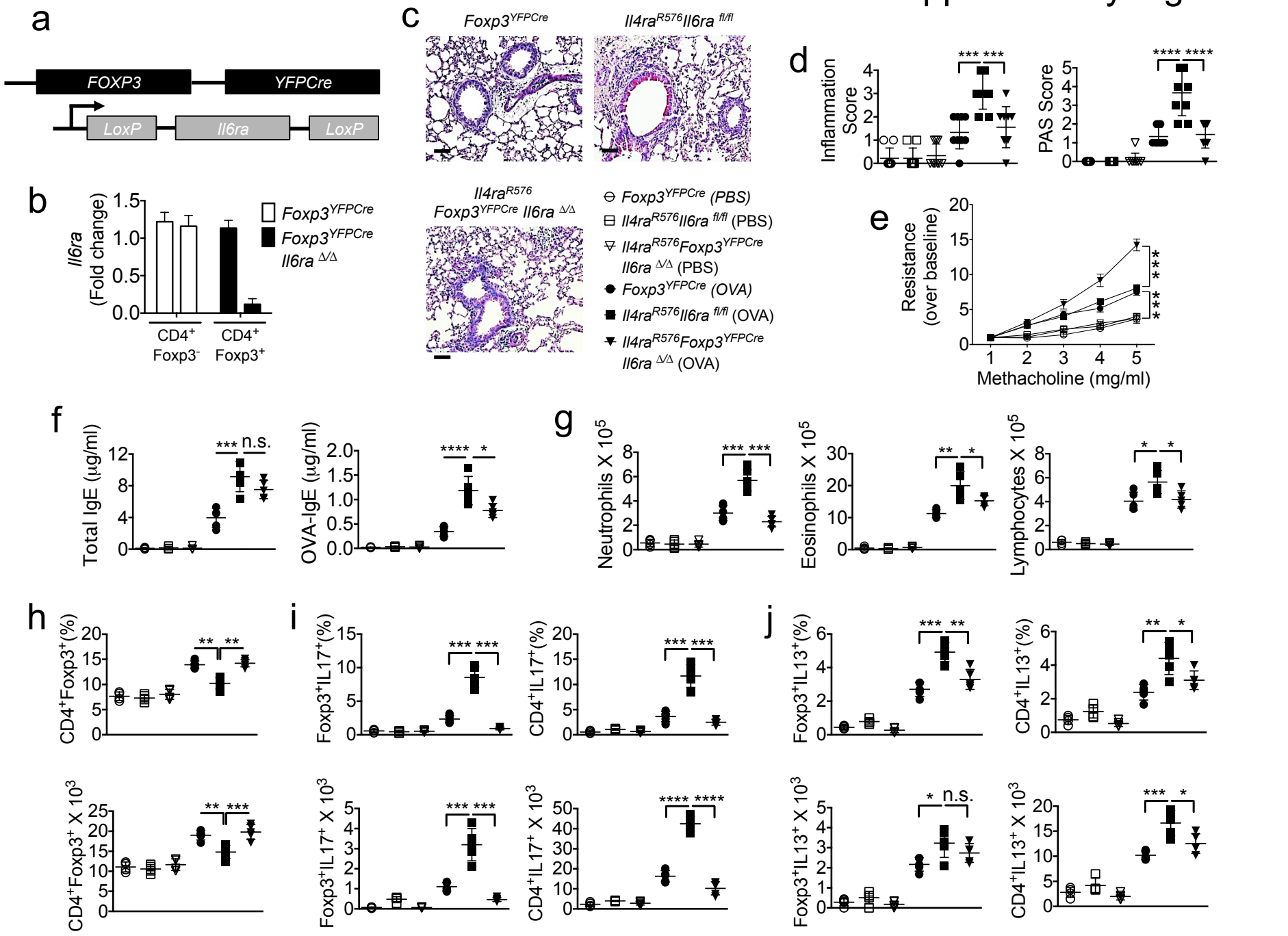

Supplementary Figure 11

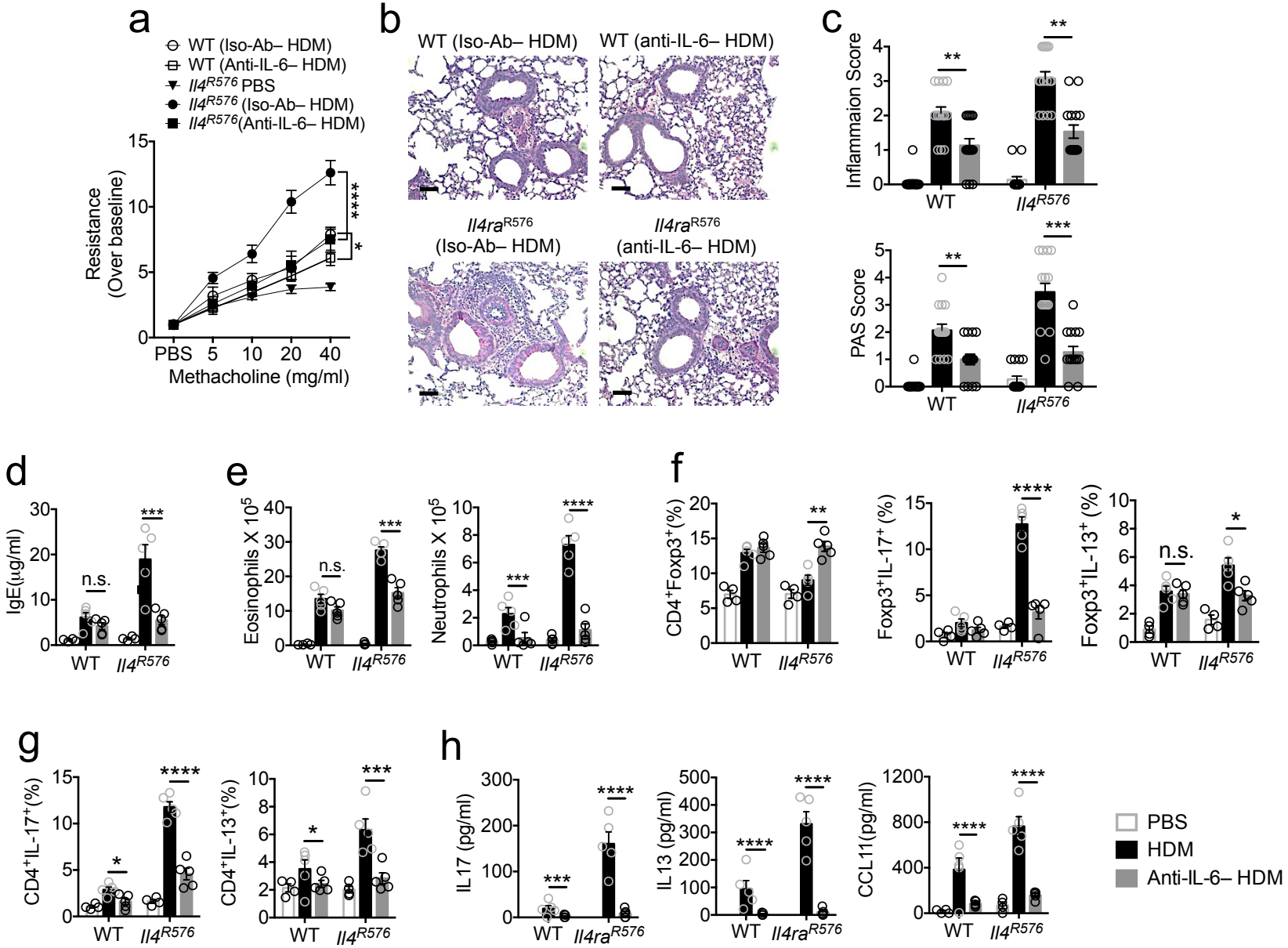

Supplementary Figure 12

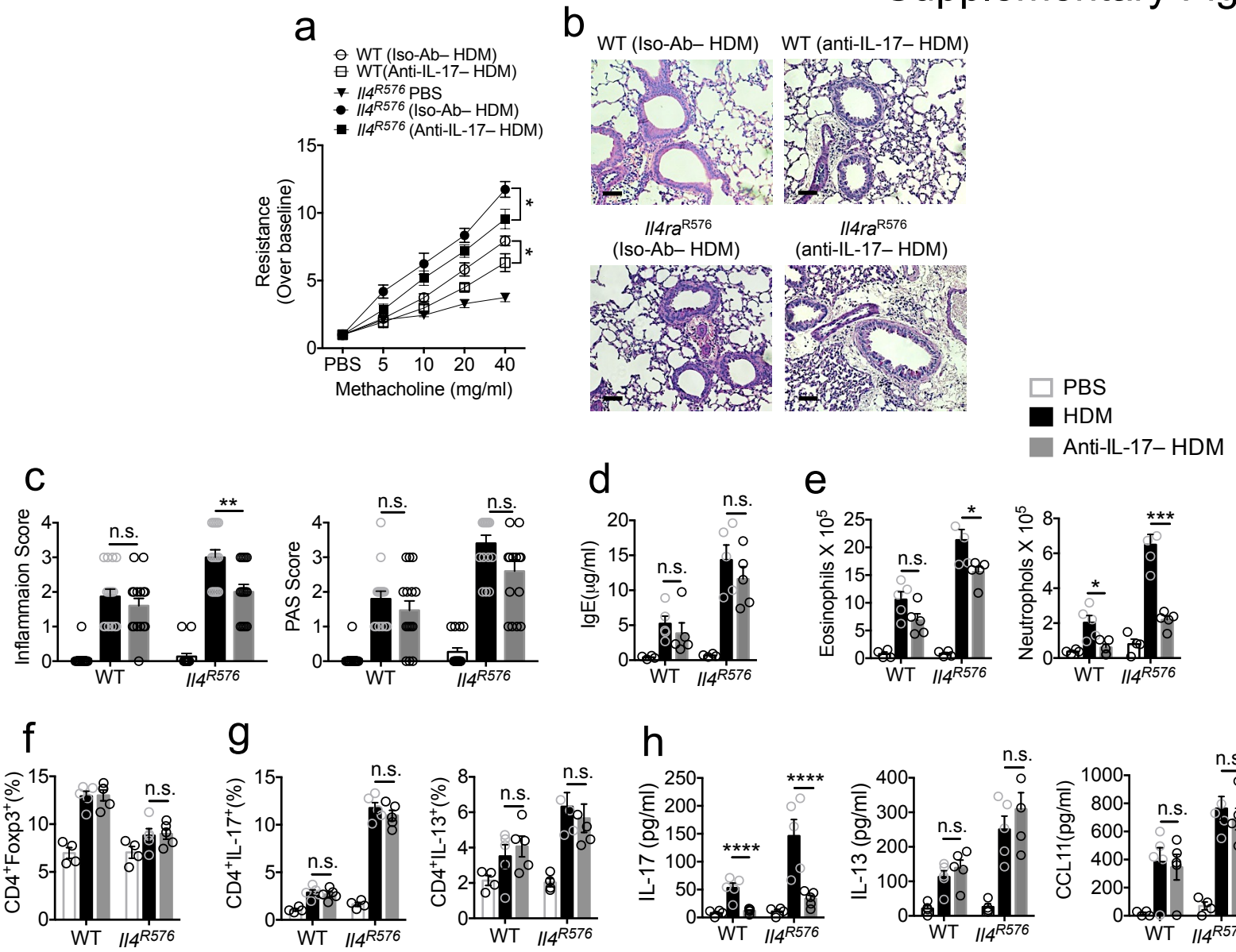

Supplementary Figure 13

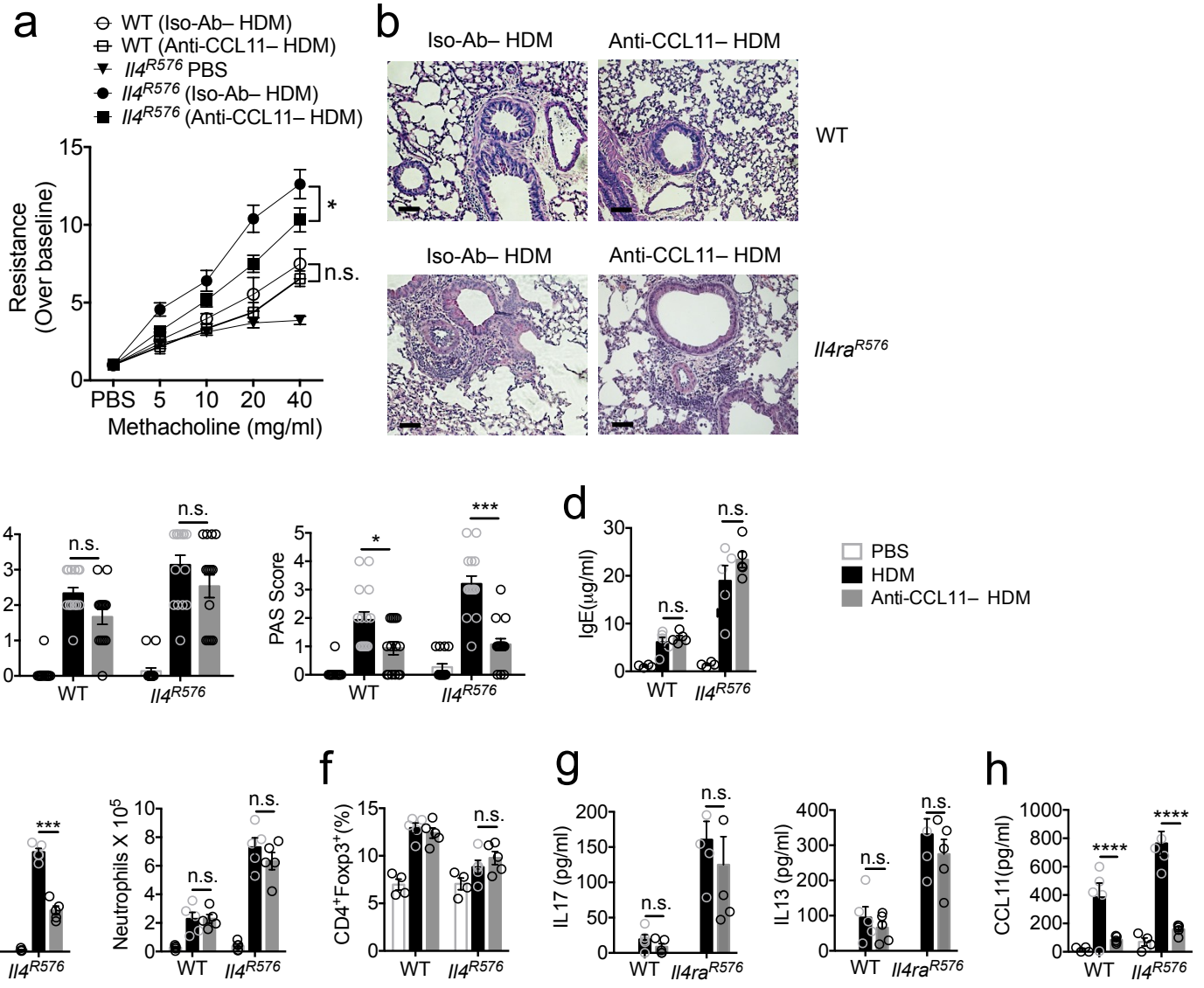

Supplementary Figure 14

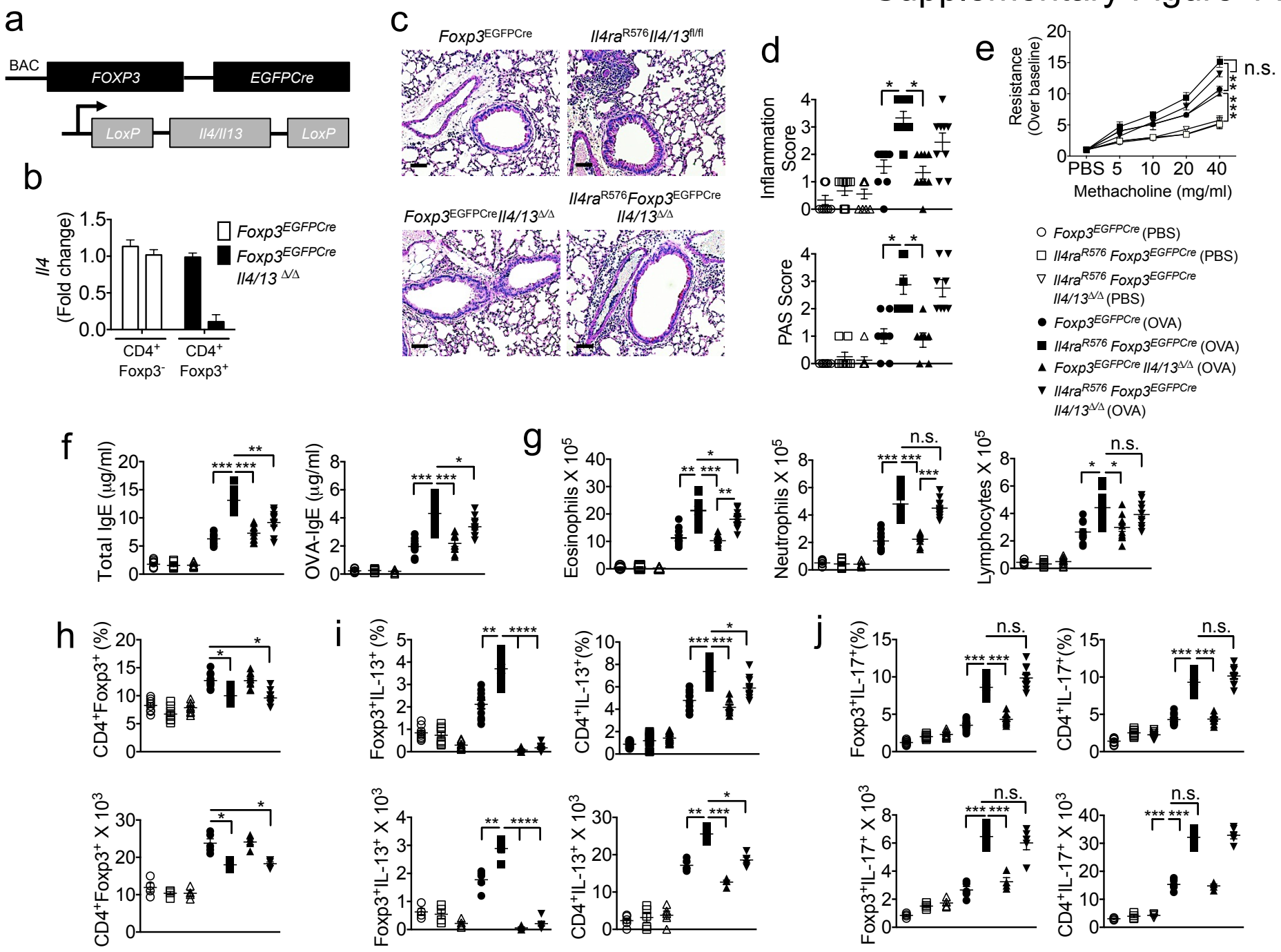

Supplementary Figure 15

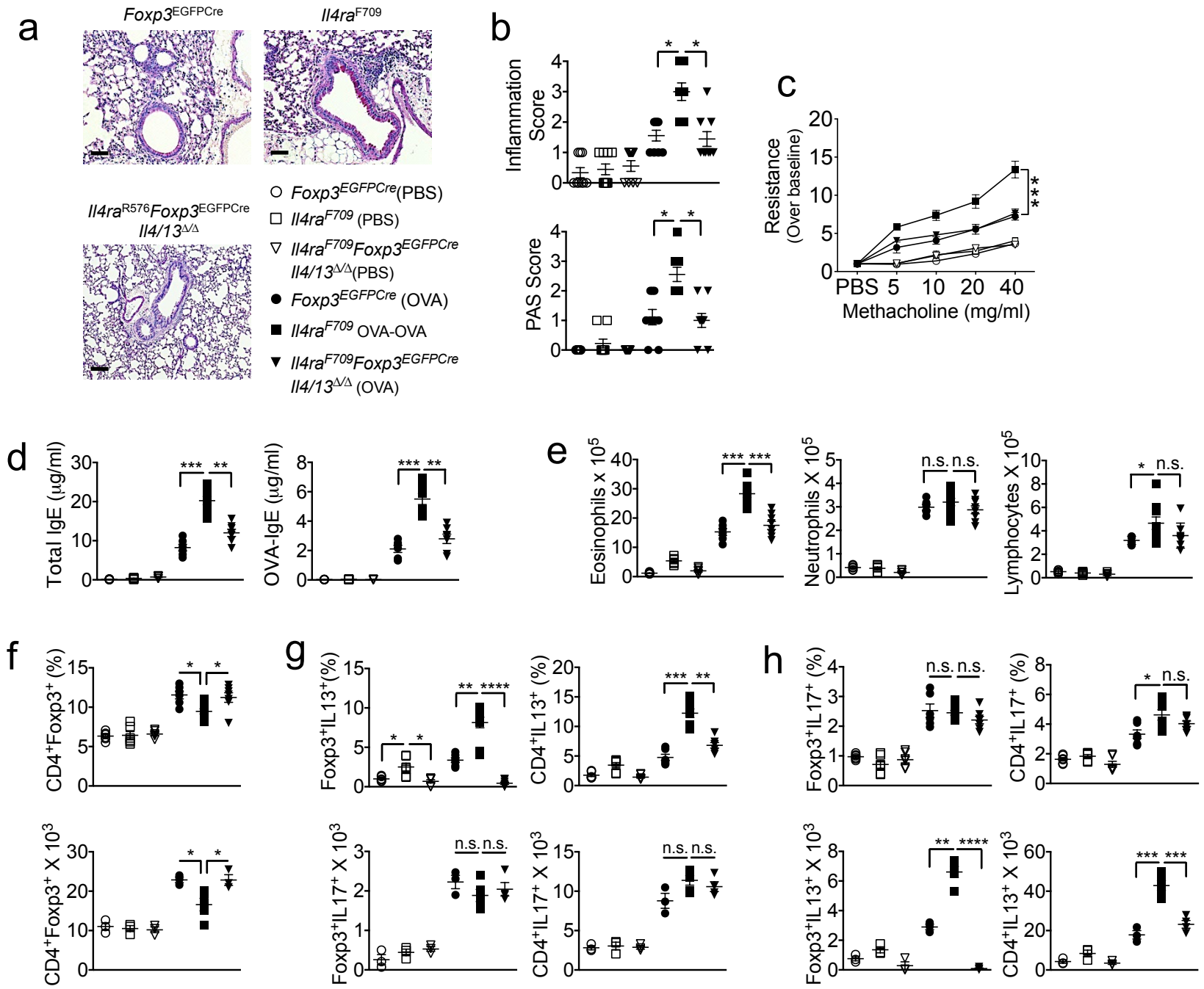

Supplementary Figure Legends

Supplementary Figure 1 *Il4ra*^{R576} polymorphism promotes the acquisition by lung tissue T_{reg} cells of T_H2 and T_H17 cell-like phenotypes. (**a,b**) Flow cytometric analysis of IL-17 vs. IL-13 (**a**) and IL-6 vs. IL-17 (**b**) cytokine expression in WT and *Il4ra*^{R576} Foxp3$^+$ T_{reg} cells within lung tissues of the HDM-treated mouse groups. (**c**) IL-4, IL-5, IL-13, IL-17 and IFN-γ cytokine levels in BAL fluids of the respective mouse groups (*n* = 5 mice for PBS- and 6 mice for HDM-treated groups). (**d–g**) Flow cytometric analysis, cell frequencies and absolute numbers of GATA3 (**d,e**) and RORγt (**f,g**) expression in CD4$^+$ Foxp3$^-$ T_{conv} and CD4$^+$ Foxp3$^+$ T_{reg} cells within lung tissue of the same mouse groups shown in **c** (*n* = 5 mice per group). (**h,i**) Flow cytometric analysis (**h**), cell frequencies and absolute numbers (**i**) of IL-4 and IFN-γ expression in CD4$^+$ T_{conv} and CD4$^+$ Foxp3$^+$ T_{reg} cells in lung tissues of the same mouse groups shown in **c** (*n* = 5 mice per group). Each dot represents one mouse. Data represent means ± s.e.m. from one experiment. **P* < 0.05, ***P* < 0.01 and ****P* < 0.001 by one-way ANOVA with Bonferroni posttest analysis.

Supplementary Figure 2 Characterization of cytokine production by CD4$^+$Foxp3$^+$ iT_{reg} and nT_{reg} cells in HDM treated *Il4ra*^{R576} mice. (**a,b**) Flow cytometric analysis (**a**) and frequencies (**b**) Helios^{high}Foxp3$^+$ and Helios^{low}Foxp3$^+$ T_{reg} cell populations in lung tissues of the respective mouse groups (*n* = 5 mice per group). (**c,d**) Flow cytometric analysis (**c**) and frequencies (**d**) of CCR6 and IL-17 co-expression in CD4$^+$Foxp3$^-$ T_{conv} and CD4$^+$Foxp3$^+$ T_{reg} cells in lung tissues of the same mouse groups shown in **b** (*n* = 5 mice per group). (**e,f**) Flow cytometric analysis (**e**) and frequencies (**f**) of CCR6, IL-17 or IL-13 vs. Helios co-expression in CD4$^+$Foxp3$^+$ T_{reg} cell populations in lung tissues of the

respective mouse groups (*n* = 5 mice per group). Each dot represents one mouse. Data represent means ± s.e.m. from one experiment. **P* < 0.05, ***P* < 0.01, ****P* < 0.001 and *****P* < 0.001 by one-way ANOVA with Bonferroni posttest analysis.

Supplementary Figure 3 Acquisition by *in vitro* derived *Il4ra*^{R576} iT$_{reg}$ cells of T$_H$17 and T$_H$2 cell-like attributes. (**a,b**) Flow cytometric analysis of RORγt (**a**) and GATA3 (**b**) in naïve WT and *Il4ra*^{R576} cells treated with anti–CD3 + anti–CD28 mAbs in the absence or presence of TGF β1 and TGF β1 + IL-4. (**c-e**) Flow cytometric analysis (**c**) and frequencies (**d,e**) of IL-4 (**d**) and IL-13 (**e**) expression in naïve T cells activated with anti-CD3 + anti-CD28 mAbs in the absence or presence of TGF β1, TGF β1 + anti–IL-4 mAb, TGF β1 + anti–IL-6 mAb and TGF β1 + IL-4 (*n* = 6 replicates). (**f–h**) Flow cytometric analysis (**f**) and frequencies (**g,h**) of IL-9 expression in CD4$^+$ Foxp3$^-$ T$_{conv}$ (**g**) and CD4$^+$Foxp3$^+$ T$_{reg}$ cell populations (**h**) within naïve T cells activated with anti–CD3 + anti–CD28 mAbs in the absence or presence of TGF β1 or TGF β1 + IL-4 (*n* = 5 replicates). Data represent means ± s.e.m. from two independent experiments. ****P* < 0.001 by one-way ANOVA with Bonferroni posttest analysis.

Supplementary Figure 4 *Il4*^{R576} nT$_{reg}$ cells exhibit comparable phenotypic and functional characterization to the WT counterparts. (**a**) Flow cytometric analysis of WT–CD4$^+$GFP$^-$ T$_{conv}$ and WT– or *Il4*^{R576}– CD4$^+$GFP$^+$Nrp1$^+$ T$_{reg}$ cells purity after purification by MACS bead and FACS. (**b,c**) Representative flow cytometric analysis (**b**) and frequencies (**c**) of proliferating WT–CD4$^+$ T (T$_{eff}$) cells co-cultured with WT or *Il4ra*^{R576} Nrp1$^+$CD4$^+$Foxp3$^+$ nT$_{reg}$ cells added at the indicated ratios. Cultured cells were stimulated with anti–CD3 + anti–CD28 mAbs in the absence or presence of recombinant IL-4 or IL-4 and anti-IL-6 mAb and assessed for their proliferation by the dilution of a

proliferative dye (*n* = 3 replicates). (**d,e**) Flow cytometric analysis (**d**) and frequencies (**e**) of IL-13 and IL-17 production by Nrp1^{+}CD4^{+}Foxp3^{+} nT$_{reg}$ cells that were isolated from spleens of naïve WT or *Il4ra*^{R576} mice and stimulated in culture with anti–CD3 + anti–CD28 mAbs in the absence or presence of recombinant IL-4 (*n* = 4 replicates). (**e,f**) flow cytometric analyses (**f**) and quantification (**g**) of IL-13 and IL-17 production by naïve CD4^{+}CD62L^{+}CD44^{-} T$_{conv}$ isolated from spleen of naïve WT or *Il4ra*^{R576} mice after culture with anti–CD3 + anti–CD28 mAb in the absence or presence of recombinant IL-4 (*n* = 5 replicates). Data represent means ± s.e.m. from two independent experiments. **P* < 0.05 and ****P* < 0.001 by one-way ANOVA with Bonferroni posttest analysis. For suppression analyses by repeated measures two-way ANOVA.

Supplementary Figure 5 Antigen–specific *Il4ra*^{R576} iT$_{reg}$ cells fail to protect against allergic airway inflammation. (**a**) Schema of the experimental design. *In vitro* derived WT or *Il4ra*^{R576} *Thy1.1*$^{+}$*DO11.10*$^{+}$*Rag2*$^{-/-}$Foxp3^{EGFP+} iT$_{reg}$ cells were adoptively transferred to OVA–sensitized *Thy1.2*$^{+}$*Il4ra*^{R576} mice prior to challenge with nebulized OVA. (**b**) PAS staining of lung sections isolated from the respective recipient mice (20×, scale bar 50 μm). (**c**) Inflammation and PAS scores (*n* = 10 counts per field-of-view) (**d**) absolute numbers of lung tissue eosinophils and neutrophils and (**e**) Methacholine–induced AHR in the respective mouse groups. (**f**) Frequencies and absolute numbers of endogenous (Thy1.2^{+}) IL-13 and IL-17 producing CD4^{+}Foxp3^{-} T$_{eff}$ and CD4^{+}Foxp3^{+} T$_{reg}$ cells in the lung tissues of the mouse groups shown in **d**. (**g,h**) Flow cytometric analysis of transferred CD4^{+}EGFP^{+} iT$_{reg}$ cells (**g**), DO11.10^{+} EGFP^{+} (iT$_{reg}$) and DO11.10^{+} EGFP^{-} (exT$_{reg}$) cells gated on Thy1.1^{+} population (**h**), all recovered from lung tissues of recipients of the mouse groups shown in **d**. (**i**) Absolute numbers of transferred iT$_{reg}$ and

exT_{reg} cells in lung tissues of the recipients. (**j**) Flow cytometric analysis and absolute numbers of IL-13 and IL-17 producing iT_{reg} and exT_{reg} cells within Thy1.1$^+$ population (*n* = 6 mice per group for **c–j**). Data represent means ± s.e.m. from 2 independent experiments. **P* < 0.05, ***P* < 0.01, ****P* < 0.001 and *****P* < 0.0001 by one-way ANOVA with Bonferroni posttest analysis. For AHR analysis, ***P* < 0.01 and ****P* < 0.001 by repeated measures two-way ANOVA.

Supplementary Figure 6 IL-4Rα-R576 activates GRB2-coupled MAPK cascades. (**a**) Binding of GRB2 and STAT6 in human PBMC lysates to the indicated biotinylated human IL-4Rα peptides as revealed by immunoblotting and quantified by densitometry (*n* = 3 replicates). (**b,c**) Time course of MAPK activation in *Il4ra*^{R576} and WT splenocytes stimulated with IL-4 for the indicated times and probed for p-c-Raf, p-ERK1/2 (**b**), p-MKK3/MKK6, p-P38 (**c**) and their corresponding non-phosphorylated proteins. (**d**) IL-4Rα-R576-mediated activation of ERK1/2 but not p38 MAPK is c-Raf-dependent. Cell lysates of IL-4–treated WT, *Il4ra*^{R576} or c-Raf inhibitor (c-Raf-Inh)-treated *Il4ra*^{R576} splenocytes were immunoblotted for the respective unmodified and phosphorylated proteins. (**e**) RT-PCR analysis of *Il6* transcripts in WT and *Il4ra*^{R576} splenocytes either untreated or treated with IL-4 in the presence of graded concentrations of p38-Inh (*n* = 3 replicates). (**f,g**) IL-4Rα-R576 mediates sustained NF-κB p65 phosphorylation in an ERK1/2-dependent manner. Splenocytes were stimulated with IL-4 in the absence (**f**) or presence (**g**) of MEK-Inh and immunoblotted for NF-κB p-p65 and p65. (**h**) IL-6 production in the cultures of differentiated iT_{reg} cells for the indicated treated groups (*n* = 3 replicates). (**i**) Flow cytometric analysis of WT and *Il4ra*^{R576} iT_{reg} cells differentiated from naïve CD4$^+$ T_{conv} cells in the presence of MEK-Inh (50 μM) or p38-Inh (10 μM),

anti-IL-4 or anti–IL-6 mAb, as indicated. (**j**) IL-17 and IL-13 expression in WT and *Il4ra*^{R576} iT$_{reg}$ cells treated as in (**j**). Data represent means ± s.e.m. from 2–3 independent experiments. ***P < 0.001 and ****P < 0.0001 by one-way ANOVA with Bonferroni posttest analysis.

Supplementary Figure 7 IL-4Rα-R576 mediates sustained STAT3 activation in T cells and BMDM in an IL-6–dependent manner. (**a**) Flow cytometric analysis and MFI (right panel) of pSTAT3 expression in WT and *Il4ra*^{R576} naïve CD4$^+$ T cells stimulated with IL-4 in the absence or presence of non–specific IgG or anti–IL-6 mAb for 1 h or indicated times. (**b,c**) MFI of pSTAT3 (**b**) and pSTAT6 (**c**) in WT and *Il4ra*^{R576} naïve CD4$^+$ T cells stimulate with IL-6 or IL-4 respectively. (**d**) Flow cytometric analysis and MFI (right panel) of pSTAT3 in WT and *Il4ra*^{R576} BMDM stimulated with IL-4 in the presence of non–specific IgG or anti–IL-6 mAb, for 1 h or indicated times. (**e**) MFI of pSTAT3 in WT and *Il4ra*^{R576} BMDM treated with IL-13 for the indicated times (n = 5 replicates for **a–e**). (**f**) RT-PCR analysis of *Ccl11* transcripts in WT and *Il4ra*^{R576} BMDM with indicated treatment. (**g**) ChIP analysis of STAT3 and STAT6 occupancy on *Ccl11* promoter in WT or *Il4ra*^{R576} BMDM either untreated or treated for 2 hr with IL-4 or IL-4 + anti–IL-6. (**h**) RT-PCR analysis of *Ccl11* transcripts in scrambled- or *Stat3* siRNA- treated BMDM either untreated or treated with IL-4 (30 min) (n = 3 replicates for **h–j**). (**i**) Representative STAT3 protein expression in scrambled- or *Stat3* siRNA treated BMDM, determined by immunoblotting. Results represent means ± s.e.m. from 1–2 independent experiments. ***P < 0.001 by one-way ANOVA with Bonferroni posttest analysis.

Supplementary Figure 8 Gating strategy of identification of T$_{reg}$ cell subpopulations in peripheral blood mononuclear cells (PBMC) of asthmatic human subjects. PBMCs of

asthmatic *Q576/Q576* and *R576/R576* subjects were analyzed by flow cytometry. Gated $CD4^+Foxp3^+$ T cells were further analyzed for Helios v.s. CCR6 and CCR6 v.s. IL-17 expression, as shown.

Supplementary Figure 9 Characterization of allergic airway inflammation in WT and *Il4ra*^{R576} mice with T_{reg} cell lineage-specific deletion of *Rorc*. (**a**) Scheme for the generation of *Foxp3*^{YFPCre}*Rorc*$^{\Delta/\Delta}$ mice. (**b**) RT-PCR analysis of *Rorc* mRNA transcripts in $CD4^+Foxp3^-$ T_{conv} and $CD4^+Foxp3^+$ T_{reg} cells of *Foxp3*^{YFPCre} and *Foxp3*^{YFPCre}*Rorc*$^{\Delta/\Delta}$ mice (*n* = 3 mice). (**c**) Absolute numbers of $CD4^+Foxp3^+$ T_{reg} cells in lung tissues of the respective mouse groups (**d**) Absolute numbers of IL-17 producing $CD4^+Foxp3^+$ T_{reg} and $CD4^+Foxp3^-$ T_{conv} cells. (**e**) IL-17 concentrations in BAL fluids of the respective mouse groups. (**f**) Absolute numbers of CCR6-expressing $CD4^+Foxp3^+$ T_{reg} and $CD4^+Foxp3^-$ T_{conv} cells. (**g**) Absolute numbers of IL-13 producing $CD4^+Foxp3^+$ T_{reg} and $CD4^+Foxp3^-$ T_{conv} cells. (**h**) IL-13 concentrations in BAL fluids of the respective mouse groups within lung tissues of the respective mouse groups (*n* = 4 mice for PBS- and 5 mice for OVA–treated groups for **c–h**). Each dot represents one mouse. Results represent means ± s.e.m. from one to two experiments. **P* < 0.05, ***P* < 0.01, ****P* < 0.001 and ****P* < 0.001 by one-way ANOVA with Bonferroni posttest analysis.

Supplementary Figure 10 Specific deletion of *Il6ra* in $Foxp3^+$ T_{reg} cells of *Il4ra*^{R576} mice reduces induced airway inflammation to those of WT counterparts. (**a**) Scheme for the generation of *Foxp3*^{YFPCre}*Il6ra*$^{\Delta/\Delta}$ mice. (**b**) RT-PCR analysis of *Il6ra* mRNA transcripts in sorted $CD4^+Foxp3^-$ T_{conv} and $CD4^+Foxp3^+$ T_{reg} cells of *Foxp3*^{YFPCre} and *Foxp3*^{YFPCre}*Il6ra*$^{\Delta/\Delta}$ mice (*n* = 3 mice). (**c**) PAS staining of lung sections of *Foxp3*^{YFPCre}, *Il4ra*^{R576}*Il6ra*$^{fl/fl}$, *Il4ra*^{R576}*Foxp3*^{EGFPCre}*Il6ra*$^{\Delta/\Delta}$ mice immunized and challenged with OVA

(20×, scale bar 50 μm). (**d**) Inflammation and PAS scores (*n* = 11 counts per field-of-view). (**e**) Methacholine–induced AHR. (**f**) Total and OVA–specific serum IgE concentrations. (**g**) Frequencies of lung tissue eosinophils, neutrophils and lymphocytes. (**h–j**) Frequencies and absolute numbers of $Foxp3^+$ T_{reg} cells (**h**), IL-13 (**i**) and IL-17 (**j**) producing $Foxp3^+T_{reg}$ and $CD4^+T_{conv}$ cells in lung tissues of respective mouse groups. Results represent means ± s.e.m. from one experiment (*n* = 4 for PBS- and 5 for OVA–treated groups for **e–j**). **P* < 0.05, ***P* < 0.01, ****P* < 0.001 and *****P* < 0.0001 by one-way ANOVA with Bonferroni posttest analysis. For AHR analyses, ****P* < 0.001 by repeated measures two-way ANOVA.

Supplementary Figure 11 Treatment with a neutralizing anti–IL-6 mAb abrogated the aggravated HDM-induced airway inflammation and AHR in *Il4ra*^{R576} mice. (**a**) Methacholine-induced AHR in PBS- and HDM-treated WT and *Il4ra*^{R576} mice that received either anti–IL-6 or isotype control mAb prior to antigen-challenge. (**b**) PAS staining of lung sections (20×, scale bar 50 μm). (**c**) Inflammation and PAS scores (*n* = 10 counts per field-of-view). (**d**) Total serum IgE concentration. (**e**) Absolute numbers of lung tissue eosinophils and neutrophils. (**f**) Frequencies of $CD4^+Foxp3^+$, $Foxp3^+IL\text{-}17^+$ and $Foxp3^+IL\text{-}13^+$ T_{reg} cells in lung tissue of the respective groups. (**g**) Frequencies of lung tissue $CD4^+IL\text{-}17^+$ and $CD4^+IL\text{-}13^+$ T_{conv} cells. (**h**) IL-17, IL-13 and CCL11 cytokines levels in BAL fluids of respective treated groups (*n* = 4 for PBS- and 5 for HDM-treated groups). Data represent means ± s.e.m. from two independent experiments. **P* < 0.05, ***P* < 0.01, ****P* < 0.001 and *****P* < 0.0001 by one-way ANOVA with Bonferroni posttest analysis. For AHR analyses, **P* < 0.05 and *****P* < 0.0001 by repeated measures two-way ANOVA.

Supplementary Figure 12 Treatment with a neutralizing anti–IL-17 mAb partially reverses the augmentation in HDM-induced airway inflammation and AHR in *Il4ra*^{R576} mice. Methacholine-induced AHR in PBS and HDM-treated WT and *Il4ra*^{R576} mice that received either anti–IL-17 or isotype control mAb prior to antigen-challenge. (**b**) PAS staining of lung sections (20×, scale bar 50 μm). (**c**) Inflammation and PAS scores (*n* = 10 counts per field-of-view). (**d**) Total serum IgE concentration. (**e**) Absolute numbers of lung tissue eosinophils and neutrophils. (**f**) Frequencies of lung tissue Foxp3$^+$ T_{reg} cells. (**g**) Frequencies of lung tissue CD4$^+$IL-17$^+$ and CD4$^+$IL-13$^+$ T_{conv} cells. (**h**) IL-17, IL-13 and CCL11 cytokines levels in BAL fluids of respective treated groups (*n* = 4 for PBS- and 5 for HDM-treated groups). Data represent means ± s.e.m. from two independent experiments. **P* < 0.05 and ***P* < 0.01 by one-way ANOVA with Bonferroni posttest analysis. For AHR analyses, **P* < 0.05 by repeated measures two-way ANOVA.

Supplementary Figure 13 Anti-CCL11 partially inhibited HDM-induced airway inflammation in WT and *Il4ra*^{R576} mice. (**a**) Methacholine-induced AHR in PBS or HDM-treated WT and *Il4ra*^{R576} mice that received anti-CCL11 or isotype antibody prior to antigen-challenge. (**b**) PAS staining of lung sections (20×, scale bar 50 μm). (**c**) Inflammation and PAS scores (*n* = 10 counts per field-of-view). (**d**) Frequencies of lung tissue eosinophils and neutrophils and total serum IgE concentration. (**e**) Frequencies of Foxp3$^+$ T_{reg} cells. (**f**) IL-17 and IL-13 cytokine levels in BAL fluids in the respective groups. (**g**) CCL11 levels in BAL fluids of respective groups. (*n* = 3 mice for PBS- and 5 mice for HDM-treated groups). Data represent means ± s.e.m. from one experiment. **P* < 0.05, **P < 0.01, ****P* < 0.001 and *****P* < 0.0001 by one-way ANOVA with Bonferroni posttest analysis. For AHR analyses, *P < 0.05 by repeated measures two-way ANOVA.

Supplementary Figure 14 Specific deletion of *Il4/Il13* in Foxp3$^+$ T_{reg} cells was not sufficient to ameliorate aggravated airway inflammation in *Il4ra*^{R576} mice. (**a**) Scheme for the generation of *Foxp3*^{EGFPCre}*Il4/13*$^{\Delta/\Delta}$ mice. (**b**) RT-PCR analysis of *Il4* mRNA transcripts in sorted CD4$^+$Foxp3$^-$ T_{conv} and CD4$^+$Foxp3$^+$ T_{reg} cells of *Foxp3*^{EGFPCre} and *Foxp3*^{EGFPCre}*Il4/13*$^{\Delta/\Delta}$ mice (*n* = 3 mice). (**c**) PAS staining of lung sections of *Foxp3*^{EGFPCre}, *Il4ra*^{R576}*Il4/1Il13*$^{fl/fl}$, *Foxp3*^{EGFPCre}*Il4/1Il13*$^{\Delta/\Delta}$ and *Il4ra*^{R576}*Foxp3*^{EGFPCre}*Il4/1Il13*$^{\Delta/\Delta}$ mice immunized and challenged with OVA (20×, scale bar 50 μm). (**d**) Inflammation and PAS scores (*n* = 10 counts per field-of-view). (**e**) Methacholine–induced AHR. (**f**) Total and OVA–specific serum IgE concentrations. (**g**) Frequencies of lung tissue eosinophils, neutrophils and lymphocytes. (**h–j**) Frequencies and absolute numbers of CD4$^+$Foxp3$^+$ T_{reg} cells (**h**), IL-13 (**i**) and IL-17 (**j**) producing CD4$^+$Foxp3$^+$ T_{reg} and CD4$^+$Foxp3$^-$ T_{conv} cells in lung tissues of the respective mouse groups. Data represent means ± s.e.m. from two independent experiments (*n* = 7 mice for PBS- and 10 mice for OVA-treated groups). **P* < 0.05, ***P* < 0.01, ****P* < 0.001 and *****P* < 0.0001 by one-way ANOVA with Bonferroni posttest analysis. For AHR analyses, ***P* < 0.05 and ****P* < 0.001 by repeated measures one-way ANOVA.

Supplementary Figure 15 Specific deletion of *Il4/Il13* in Foxp3$^+$ T_{reg} cells rescued aggravated airway inflammation in *Il4ra*^{F709} mice. (**a**) PAS staining of lung sections of *Foxp3*^{EGFPCre}, *Il4ra*^{F709}*Il4/1Il13*$^{fl/fl}$, *Foxp3*^{EGFPCre}*Il4/1Il13*$^{\Delta/\Delta}$ and *Il4ra*^{F709}*Foxp3*^{EGFPCre}*Il4/1Il13*$^{\Delta/\Delta}$ mice immunized and challenged with OVA (20×, scale bar 50 μm). (**b**) Inflammation and PAS scores (*n* = 10 counts per field-of-view). (**c**) Methacholine-induced AHR. (**d**) Total and OVA-specific serum IgE concentrations. (**e**) Frequencies of lung tissue eosinophils, neutrophils and lymphocytes. (**f–h**) Frequencies

and absolute numbers of $CD4^+Foxp3^+$ T_{reg} cells (**f**), IL-13 (**g**) and IL-17 (**h**) producing $CD4^+Foxp3^+$ T_{reg} and $CD4^+$ $Foxp3^-$ T_{conv} cells in lung tissues of the respective mouse groups. Data represent means ± s.e.m. from two independent experiments (n = 7 mice for PBS- and 10 mice for OVA-treated groups). *P < 0.05, **P < 0.01, ***P < 0.001 and ****P < 0.0001 by one-way ANOVA with Bonferroni posttest analysis. For AHR analysis, ***P < 0.001 by repeated measures two-way ANOVA.

Supplemental Table 1 Demographic Characteristics and genotype of enrolled non-asthmatic study participants.

Subject-Genotype	Age (Y)	Sex
1-Q576/Q576	22	M
2-Q576/Q576	28	M
3-Q576/Q576	31	M
4-Q576/Q576	32	M
5-Q576/Q576	36	F
6-Q576/Q576	24	F
7-Q576/Q576	26	F
8-Q576/Q576	27	F
9-Q576/Q576	29	M
10-Q576/Q576	21	M
11-Q576/Q576	25	M
12-Q576/Q576	34	M
13-Q576/Q576	46	M
14-Q576/R576	30	M
15-Q576/R576	27	M
16-Q576/R576	26	F
17-Q576/R576	21	M
18-Q576/R576	41	M
19-R576/R576	37	M
20-R576/R576	36	M
21-R576/R576	43	M

Supplemental Table 2 Demographics, genotype and clinical characteristics of enrolled asthmatic study participants.

Subject-Genotype	Age (Y)	Sex	Asthma Severity
1-Q576/Q576	13	M	Intermittent
2-Q576/Q576	14	M	Persistent Mild
3-Q576/Q576	14	F	Persistent Mild
4-Q576/Q576	8	F	Persistent Mild
5-Q576/Q576	11	F	Intermittent
6-Q576/Q576	10	M	Persistent Severe
7-Q576/Q576	17	M	Persistent Moderate
8-Q576/Q576	16	M	Persistent Mild
9-Q576/Q576	11	M	Intermittent
10-Q576/Q576	10	F	Persistent Moderate
11-Q576/Q576	16	M	Intermittent
12-Q576/Q576	12	F	Persistent Mild
13-Q576/Q576	11	M	Persistent Moderate
14-Q576/Q576	6	F	Persistent Moderate
15-Q576/Q576	40	F	Persistent Mild
16-Q576/Q576	34	F	Persistent Mild
17-Q576/Q576	27	F	Persistent Mild

18-Q576/Q576	33	F	Persistent Moderate
19-Q576/Q576	3	F	Persistent Mild
20-Q576/R576	14	F	Persistent Moderate
21-Q576/R576	13	F	Persistent Mild
22-Q576/R576	15	F	Persistent Moderate
23-Q576/R576	10	M	Persistent Moderate
24-R576/R576	9	F	Persistent Moderate
25-R576/R576	26	F	Persistent Moderate
26-R576/R576	11	F	Persistent Moderate
27-R576/R576	12	M	Persistent Severe
28-R576/R576	12	M	Persistent Severe
29-R576/R576	14	M	Persistent Severe
30-R576/R576	11	M	Persistent Severe

Asthma severity was classified as follows: Intermittent (symptoms < 2 days/week), Mild (symptoms> 2 days/week but not daily), Moderate (daily symptoms), and Severe (symptoms throughout the day). An average asthma severity score was calculated for each group by assigning intermittent asthma a score of 1, mild persistent asthma a score of 2, moderate persistent asthma a score of 3 and severe asthma a score of 4. The average severity score for asthmatics homozygous for the Q576 residue (*n* =1 9) was 2.16 ± 0.19 and those heterozygous or homozygous for the R576 reside (n=11) was 3.27 ± 0.19 (p=0.0007 by Student's unpaired two tailed t test). The two groups were otherwise not significantly different by age (*p* = 0.40 by Student's unpaired two tailed t test) or sex (0.69 by Fisher's exact test).